
LATENT NONLINEAR DENOISING SCORE MATCHING FOR ENHANCED LEARNING OF STRUCTURED DISTRIBUTIONS

A PREPRINT

Kaichen Shen
 School of Mathematics
 Georgia Institute of Technology
 Atlanta, GA
 kshen77@gatech.edu

Wei Zhu
 School of Mathematics
 Georgia Institute of Technology
 Atlanta, GA
 weizhu@gatech.edu

December 6, 2025

ABSTRACT

We present latent nonlinear denoising score matching (LNDSM), a novel training objective for score-based generative models that integrates nonlinear forward dynamics with the VAE-based latent SGM framework. This combination is achieved by reformulating the cross-entropy term using the approximate Gaussian transition induced by the Euler–Maruyama scheme. To ensure numerical stability, we identify and remove two zero-mean but variance exploding terms arising from small time steps. Experiments on variants of the MNIST dataset demonstrate that the proposed method achieves faster synthesis and enhanced learning of inherently structured distributions. Compared to benchmark structure-agnostic latent SGMs, LNDSM consistently attains superior sample quality and variability.

Keywords Score-based generative modeling · structure-preserving models · denoising score-matching · latent space · learning from scarce data

1 Introduction

Score-based generative models (SGMs) provide a flexible framework for learning complex data distributions by estimating the score of a diffusion process that links a simple reference distribution (such as Gaussian) to the data distribution [10, 22]. Compared to generative adversarial networks (GANs) [8] and variational autoencoders (VAEs) [13], SGMs achieve high sample quality and avoid adversarial training instabilities [7]. They also admit an equivalent probability flow ODE representation, placing them within the broader class of flow-based generative models [15].

In many applications, however, the target distribution exhibits inherent structural properties that are not exploited by standard generative models. Examples include group invariances in medical and scientific imaging, as well as multimodal or low-dimensional structure in dynamical and molecular systems. To incorporate such structure into generative models, specialized architectures or model adaptations must be employed. For instance, to generate distributions with intrinsic group symmetry (that is, a sample and its group-transformed copy have the same probability), symmetry is enforced in GANs through equivariant generators and discriminators [6, 3]. For SGMs, analogous constraints are imposed using group-equivariant score networks [16]. More recently, [2] proposed a more general and relaxed framework in which structure is incorporated by tailoring the reference distribution to share qualitative features with the target. This is achieved by using *nonlinear* forward dynamics driven by a structured reference measure, which can significantly enhance the learning of structured distributions.

A complementary line of work improves SGMs by moving from the data space to a lower-dimensional latent space [24, 19, 17, 4, 26]. Mapping data to a smooth latent manifold reduces the computational cost of training and sampling while often improving expressivity [19]. A representative example is latent score-based generative modeling (LSGM) [24], which combines a variational autoencoder (VAE) with an SGM that learns the prior over latent variables. In LSGM, the latent prior is trained through a VAE-induced objective in which a denoising score-matching term appears as a cross entropy between the encoder distribution and the score-based prior. This formulation, however, relies on an *linear* drift

in the latent diffusion and uses a Gaussian reference distribution, which is not tailored to structural properties of the latent distribution such as multimodality. Moreover, standard LSGM requires importance sampling in time to control variance in the training objective, which complicates both the theory and the implementation.

The goal of this work is to unify the strengths of these two directions. We introduce latent nonlinear denoising score matching (LNDSM), a new training objective that brings nonlinear diffusions into the latent SGM framework. Our approach uses the Euler–Maruyama (EM) discretization of a general nonlinear diffusion in latent space and rewrites the VAE-induced cross entropy in terms of conditional Gaussian transitions. This allows us to replace the intractable marginal score by computable conditional scores. A central technical step is identifying and removing two variance-exploding terms arising from small EM time steps; subtracting these control variates yields a numerically stable objective. The encoder, decoder, and latent score network are then trained jointly using this LNDSM loss.

We demonstrate that our proposed LNDSM enhances the modeling of structured distributions and accelerates synthesis. Experiments on multimodal and approximately group symmetric dataset—especially in low-data regimes—show that LNDSM achieves lower Fréchet inception distance (FID) [9], higher inception score (IS) [21], and significantly improved mode balance compared to LSGM, while requiring far fewer training time. These results indicate that combining structured latent reference distributions with nonlinear latent diffusions provides a powerful and efficient framework for learning structured data distributions.

2 Background and Motivation

2.1 Score-based Generative Models (SGMs)

We briefly review the score-based generative modeling through stochastic differential equations (SDEs) [22]. Consider a diffusion process $\{x_t\}_{t \in [0, T]}$, where for each $t \in [0, T]$, x_t is a \mathbb{R}^d -valued random variable. The initial state $x_0 \sim p_0 = p_{\text{data}}$ follows the unknown target data distribution. The terminal state $x_T \sim p_T$ is designed to be, or approximately follow, a simple reference distribution π (typically a Gaussian) with a known and tractable density. The goal of generative modeling is to learn p_{data} by generating new samples that are consistent with this distribution.

The forward noising process is modeled by the SDE

$$dx_t = f(x_t, t)dt + g(t)dw_t, \quad (1)$$

where $f(\cdot, t) : \mathbb{R}^d \rightarrow \mathbb{R}^d$ is the drift, $g(\cdot) : \mathbb{R} \rightarrow \mathbb{R}$ is the diffusion coefficient and w_t is the standard Wiener process. Under this dynamics, the data distribution p_0 is gradually transformed into the reference distribution $\pi \approx p_T$.

A fundamental result due to Anderson [1] establishes that, under mild regularity conditions, the forward diffusion process admits an exact time reversal in distribution. In particular, the time-reversed process is again an Itô diffusion whose drift contains an additional correction term involving the score of the marginal density. Specifically, the reverse-time SDE associated with the forward process takes the form

$$dx_t = [f(x_t, t) - g^2(t)\nabla_{x_t} \log p_t(x_t)] dt + g(t)d\bar{w}_t, \quad (2)$$

where \bar{w}_t is the standard Wiener process evolving backward from T to 0, and $\nabla_x \log p_t(x)$ denotes the *score* of the marginal distribution at time t . This reverse-time formulation was first adopted in score-based generative modeling by Song et al. [22] and forms the basis for generative sampling.

Since the score $\nabla_x \log p_t(x)$ is generally unknown, it is typically approximated by a time-dependent neural network $s_\theta(x_t, t)$, which can be trained via denoising score matching [25]:

$$\theta^* = \arg \min_{\theta} \mathbb{E}_t \left\{ \lambda(t) \mathbb{E}_{x_0} \mathbb{E}_{x_t | x_0} \left[\|s_\theta(x_t, t) - \nabla_{x_t} \log p_{0t}(x_t | x_0)\|_2^2 \right] \right\}. \quad (3)$$

Here t is sampled uniformly from $[0, T]$, $\lambda(t)$ is a positive weighting function, $x_0 \sim p_0 = p_{\text{data}}$ and $x_t \sim p_{0t}(\cdot | x_0)$. Transition density $p_{0t}(x_t | x_0)$ admits a closed-form expression only when the forward diffusion is an *Ornstein–Uhlenbeck (OU) process*, that is, when the drift is linear in x_t of the form $f(x_t, t) = -\alpha(t)x_t$. In this case, the forward process is Gaussian with explicitly known mean and covariance, which makes the denoising score matching objective tractable. This linear (OU) structure is therefore a key prerequisite for the practical implementation of classical denoising score matching in SGMs.

After training, the intractable score $\nabla_{x_t} \log p_t(x_t)$ in the reverse-time SDE is replaced by its neural approximation $s_{\theta^*}(x_t, t)$. Numerical simulation of the reverse-time SDE then produces samples from the learned approximation of the target distribution.

2.2 Latent Score-based Generative Models (LSGMs)

We next review the extension of SGM to a latent space, known as the latent score-based generative models [24]. By operating in a lower-dimensional latent space, LSGM improves both the synthesis speed and the expressivity of standard SGMs. Conceptually, LSGM combines a variational autoencoder (VAE) with score-based generative modeling by learning the latent prior through an SGM rather than prescribing it a priori. Specifically, the encoder $q_\phi(z_0|x)$ maps a data point x in the original space to a distribution over a latent variable z_0 in a lower-dimensional latent space, while the decoder $p_\psi(x|z_0)$ maps z_0 back to a distribution over x . The parameters ϕ and ψ are learned jointly from data.

In a standard VAE, the prior of the latent variable z_0 is fixed in advance, typically as a standard Gaussian $\mathcal{N}(0, I)$. In contrast, LSGM learns the latent prior using score-based generative modeling in the latent space. Specifically, i.i.d. samples from the data distribution are first mapped to the latent space and treated as samples from a latent target distribution, which is approximated by an SGM. This learned prior is denoted as $p_\theta(z_0)$, where θ denotes the parameters of the score network. The encoder, decoder, and score network parameters $\{\phi, \theta, \psi\}$ are trained jointly. For a data point x , the training loss is given by

$$\begin{aligned}\mathcal{L}(x, \phi, \theta, \psi) &= \mathbb{E}_{q_\phi(z_0|x)}[-\log p_\psi(x|z_0)] + D_{\text{KL}}(q_\phi(z_0|x) \| p_\theta(z_0)) \\ &= \mathbb{E}_{q_\phi(z_0|x)}[-\log p_\psi(x|z_0)] + \mathbb{E}_{q_\phi(z_0|x)}[\log q_\phi(z_0|x)] + \text{CE}(q_\phi(z_0|x) \| p_\theta(z_0)).\end{aligned}\quad (4)$$

In (4), the first term is the reconstruction loss, the second term is the negative encoder entropy, and the third term is the cross entropy between the prior given by the encoder and the prior learned by the SGM in the latent space. Furthermore, this cross-entropy term admits a denoising score-matching form,

$$\begin{aligned}\text{CE}(q_\phi(z_0|x) \| p_\theta(z_0)) &= \mathbb{E}_{q_\phi(z_0|x)}[-\log p_\theta(z_0)] \\ &= \mathbb{E}_t \left[\frac{g^2(t)}{2} \mathbb{E}_{q_\phi(z_t, z_0|x)} [\|s_\theta(z_t, t) - \nabla_{z_t} \log p_{0t}(z_t|z_0)\|_2^2] \right] + c,\end{aligned}\quad (5)$$

where t is uniformly sampled from $[0, T]$, $q_\phi(z_t, z_0|x) = p_{0t}(z_t|z_0)q_\phi(z_0|x)$, and c is a constant. Note that expression (5) is implementable only when the latent diffusion has a drift that is *linear* in z_t , ensuring that the transition density $p_{0t}(z_t|z_0)$ is Gaussian and tractable.

2.3 Nonlinear Denoising Score Matching (NDSM)

Another way to improve SGM is to explicitly incorporate the structural properties of the target distribution. In this subsection, we review the score-based generative modeling framework with nonlinear dynamics proposed in [2], which we refer to as NDSM-SGM. This method enhances the learning of structured distributions by introducing a reference distribution $\pi(x)$ that shares qualitative structural features with the target distribution $p_0(x)$. A Langevin dynamics that converges to the reference distribution $\pi(x)$ is then chosen as the forward noising process:

$$dx_t = -\nabla_{x_t} V(x_t)dt + \sqrt{2}dw_t, \quad V(x) := -\log(\pi(x)), \quad (6)$$

so that $\pi(x)$ is the invariant measure of the diffusion. This dynamics transports the target distribution $p_0(x)$ toward a structured reference distribution that encodes prescribed qualitative features, such as multimodality or approximate symmetries. Importantly, the reference distribution is *not required to share exactly the same structure* as the target; instead, it provides a relaxed structural bias that guides the diffusion.

Because the drift term $-\nabla_{x_t} V(x_t)$ is generally nonlinear, the transition density $p_{0t}(x_t|x_0)$ does not admit a closed-form expression, rendering classical denoising score matching inapplicable. NDSM addresses this by applying the Euler–Maruyama (EM) discretization to a general forward SDE to obtain an approximate discrete-time Markov process $\{x_n\}_{n=0}^{n_f}$, with $t_0 = 0$ and $t_{n_f} = T$:

$$x_0 \sim p_0(x), \quad (7)$$

$$\begin{aligned}x_n &\approx x_{n-1} + f(x_{n-1}, t_{n-1})\Delta t_{n-1} + g(t_{n-1})\sqrt{\Delta t_{n-1}}U_{n-1} \\ &:= \mu(x_{n-1}, t_{n-1}, \Delta t_{n-1}) + \sigma(x_{n-1}, t_{n-1}, \Delta t_{n-1})U_{n-1}, \quad 1 \leq n \leq n_f,\end{aligned}\quad (8)$$

where $\Delta t_{n-1} = t_n - t_{n-1}$ and $U_{n-1} \sim \mathcal{N}(0, I)$. When Δt_{n-1} is sufficiently small, the conditional distribution satisfies

$$p(x_n|x_{n-1}) = \mathcal{N}(x_n; \mu(x_{n-1}, t_{n-1}, \Delta t_{n-1}), \sigma^2(x_{n-1}, t_{n-1}, \Delta t_{n-1})I), \quad (9)$$

Based on this Markov approximation, NDSM replaces the intractable expected ℓ^2 error between the score network and the marginal score by a computable surrogate objective:

$$\arg \min_{\theta} \frac{1}{2} \mathbb{E}_N [\|s_\theta(x_N, t_N) - \nabla_{x_N} \log p_N(x_N)\|_2^2] = \arg \min_{\theta} \mathbb{E} [\mathcal{L}_{\theta, N}^{\text{NDSM}}], \quad (10)$$

where

$$\mathcal{L}_{\theta,N}^{\text{NDSM}} := \frac{1}{2} \|s_\theta(x_N, t_N)\|_2^2 + \frac{U_N \cdot [s_\theta(x_N, t_N) - s_\theta(\mu(x_{N-1}, t_{N-1}, \Delta t_{N-1}), t_N)]}{\sigma(x_{N-1}, t_{N-1}, \Delta t_{N-1})}.$$

Here N is a random time index, uniformly distributed over $\{1, \dots, n_f\}$ and independent of x_0 and the Gaussian noises $\{U_n\}$. This construction yields a tractable training objective for SGMs with nonlinear forward dynamics while effectively incorporating structural information through the choice of the reference distribution $\pi(x)$.

While NDSM-SGM effectively incorporates structural information through nonlinear forward dynamics, it requires simulating SDEs in the full ambient space, which leads to substantial computational cost. In contrast, LSGM achieves significant improvements in synthesis speed by operating in a lower-dimensional latent space. Moreover, in many applications the intrinsic structure of the data may be represented more naturally and compactly in the latent space than in the original data space. These considerations naturally motivate combining the structural advantages of NDSM-SGM with the computational efficiency of LSGM, leading to our proposed latent nonlinear denoising score-matching framework.

3 Nonlinear Denoising Score Matching in Latent Space

The goal of this work is to extend NDSM-SGM (section 2.3) to the latent space using the VAE-based training framework of LSGM (section 2.2). Following the same notation as LSGM, we denote the encoder by $q_\phi(z_0|x)$ and the decoder by $p_\psi(x|z_0)$. We consider a general (nonlinear) diffusion process in the latent space of the form

$$dz_t = f(z_t, t)dt + g(t)dw_t. \quad (11)$$

Using the same principle as in the NDSM framework, we impose a relaxed structural constraint on the latent diffusion by requiring it to converge to a prescribed reference distribution in the latent space. This reference distribution is designed to share *similar, but not necessarily identical*, structural characteristics with the target *latent* distribution induced by the encoder. We retain the VAE-based training objective, in analogy with (4):

$$\begin{aligned} \mathbb{E}_{x \sim p_{\text{data}}} [\mathcal{L}(x, \phi, \theta, \psi)] &= \mathbb{E}_{x \sim p_{\text{data}}} \left\{ \mathbb{E}_{q_\phi(z_0|x)} [-\log p_\psi(x|z_0)] + \mathbb{E}_{q_\phi(z_0|x)} [\log q_\phi(z_0|x)] + \mathbb{E}_{q_\phi(z_0|x)} [-\log p_\theta(z_0)] \right\} \\ &= \mathbb{E}_{x \sim p_{\text{data}}} \left\{ \mathbb{E}_{q_\phi(z_0|x)} [-\log p_\psi(x|z_0)] + \mathbb{E}_{q_\phi(z_0|x)} [\log q_\phi(z_0|x)] + \text{CE}(q_\phi(z_0|x) \| p_\theta(z_0)) \right\}. \end{aligned} \quad (12)$$

Here, the latent prior $p_\theta(z_0)$ in the cross-entropy term is now learned via NDSM-SGM in the latent space, with θ being the parameter of the latent score network. The modeling of this cross entropy term is detailed in the following subsection.

3.1 Cross Entropy Term

The main theoretical and algorithmic contribution of this work is the integration of NDSM into the cross-entropy term of the VAE training objective (12). We first show (see Lemma 1 in Appendix A for details) that the cross-entropy term $\text{CE}(q_\phi(z_0|x) \| p_\theta(z_0))$ in the loss function 12 can be expressed as

$$\begin{aligned} \text{CE}(q_\phi(z_0|x) \| p_\theta(z_0)) &= H(q_\phi(z_T|x)) + \frac{1}{2} \int_0^T g^2(t) \mathbb{E}_{q_\phi(z_t|x)} [\|\nabla_{z_t} \log q_\phi(z_t|x) - s_\theta(z_t, t)\|_2^2] dt \\ &\quad + \frac{1}{2} \int_0^T \mathbb{E}_{q_\phi(z_t|x)} \left[\left[2f(z_t, t) - g^2(t) \nabla_{z_t} \log q_\phi(z_t|x) \right]^T \nabla_{z_t} \log q_\phi(z_t|x) \right] dt, \end{aligned} \quad (13)$$

where $H(q_\phi(z_T|x))$ is the entropy of the chosen latent reference distribution. Since the latent diffusion process (11) has a nonlinear drift, the exact form of the density $q_\phi(z_t|x)$ is generally intractable. As in the NDSM framework in section 2.3, we therefore replace the intractable marginal density by a computable (local) conditional density obtained through time discretization. Specifically, we simulate the latent diffusion using the Euler–Maruyama (EM) scheme, which yields a discrete-time Markov process $\{z_n\}_{n=0}^{n_f}$, with $t_0 = 0$ and $t_{n_f} = T$:

$$z_0 \sim q_\phi(z_0|x)p_0(x), \quad (14)$$

$$\begin{aligned} z_n &\approx z_{n-1} + f(z_{n-1}, t_{n-1})\Delta t_{n-1} + g(t_{n-1})\sqrt{\Delta t_{n-1}}U_{n-1} \\ &:= \mu(z_{n-1}, t_{n-1}, \Delta t_{n-1}) + \sigma(z_{n-1}, t_{n-1}, \Delta t_{n-1})U_{n-1}, \quad 1 \leq n \leq n_f, \\ &:= \mu_{n-1} + \sigma_{n-1}U_{n-1}, \quad 1 \leq n \leq n_f, \end{aligned} \quad (15)$$

where $\Delta t_{n-1} = t_n - t_{n-1}$ is sufficiently small, and $U_{n-1} \sim \mathcal{N}(0, I)$. Introducing a random time index N , uniformly distributed over $\{0, \dots, n_f\}$, the cross-entropy term $\text{CE}(q_\phi(z_0|x)||p_\theta(z_0))$ can be approximated by:

$$\begin{aligned} \text{CE}(q_\phi(z_0|x)||p_\theta(z_0)) &\approx H(q_\phi(z_{n_f})) + \underbrace{\frac{1}{2} \mathbb{E}_{N, z_N} [g^2(t_N) \|\nabla_{z_N} \log q_\phi(z_N) - s_\theta(z_N, t_N)\|_2^2]}_{\text{(I)}} \\ &\quad + \underbrace{\frac{1}{2} \mathbb{E}_{N, z_N} \left[[2f(z_N, t_N) - g^2(t_N) \nabla_{z_N} \log q_\phi(z_N)]^T \nabla_{z_N} \log q_\phi(z_N) \right]}_{\text{(II)}} \end{aligned} \quad (16)$$

All continuous-time variables are thus replaced by their discrete-time counterparts.

The remaining task is to convert the marginal score $\nabla_{z_N} \log q_\phi(z_N)$ in (16) into the conditional score $\nabla_{z_N} \log q_\phi(z_N|z_{N-1})$, which is tractable since the conditional distribution $z_N|z_{N-1}$ is approximately Gaussian if the discretization of time is sufficiently fine. Note that the squared-norm term (I) in (16) can be expanded: the squared norm of $s_\theta(z_N, t_N)$ is computed by the score network directly, and the squared norm of $\nabla_{z_N} \log q_\phi(z_N)$ is cancelled by the corresponding term in (II) of Eq. (16). Therefore, the remaining terms containing the unknown marginal score $\nabla_{z_N} \log q_\phi(z_N)$ are:

$$A = \mathbb{E}_{N, z_N} [g^2(t_N) s_\theta(z_N, t_N) \cdot \nabla_{z_N} \log q_\phi(z_N)], \quad (17)$$

$$B = \mathbb{E}_{N, z_N} [f(z_N, t_N) \cdot \nabla_{z_N} \log q_\phi(z_N)]. \quad (18)$$

Using a derivation similar to those in [25, 22, 10], the marginal score $\nabla_{z_N} \log q_\phi(z_N)$ appearing in (17) and (18) admits an alternative expression in terms of the conditional score $\nabla_{z_N} \log q_\phi(z_N | z_{N-1})$; see Appendix B for the detailed derivations. With this representation, (17) and (18) can be written as:

$$A = \mathbb{E}_{N, z_{N-1}, z_N} [g^2(t_N) s_\theta(z_N, t_N) \cdot \nabla_{z_N} \log q_\phi(z_N | z_{N-1})], \quad (19)$$

$$B = \mathbb{E}_{N, z_{N-1}, z_N} [f(z_N, t_N) \cdot \nabla_{z_N} \log q_\phi(z_N | z_{N-1})], \quad (20)$$

where

$$\nabla_{z_N} \log q_\phi(z_N | z_{N-1}) \approx -\frac{U_{N-1}}{\sigma_{N-1}} = -\frac{U_{N-1}}{g(t_{N-1}) \sqrt{\Delta t_{N-1}}}. \quad (21)$$

Note that to have an accurate Gaussian approximation of the conditional score $\nabla_{z_N} \log q_\phi(z_N | z_{N-1})$, Δt_{N-1} must be sufficiently small. However, since the conditional score scales as $1/\sqrt{\Delta t_{N-1}}$, this choice leads to terms of large magnitude and consequently high variance.

To mitigate this issue, we identify and remove the following two dominant *mean-zero* terms from (19) and (20) via first-order Taylor expansions of $s_\theta(z_N, t_N)$ and $f(z_N, t_N)$ about (μ_{N-1}, t_N) :

$$s_\theta(\mu_{N-1}, t_N) \frac{U_{N-1}}{\sigma_{N-1}}, \quad f(\mu_{N-1}, t_N) \frac{U_{N-1}}{\sigma_{N-1}}. \quad (22)$$

These two terms are referred to as control variates in [2] due to their zero-mean property. In general, learnable coefficients can be multiplied with these control variates and added back to the training loss for variance reduction. In our setting, we simply remove them from the training loss. See Appendix B for further details. As a result, Eqs. (19) and (20), respectively, can be written as

$$- \mathbb{E}_{N, z_{N-1}, z_N} \left[g^2(t_N) \frac{U_{N-1}}{\sigma_{N-1}} [s_\theta(z_N, t_N) - s_\theta(\mu_{N-1}, t_N)] \right], \quad (23)$$

$$- \mathbb{E}_{N, z_{N-1}, z_N} \left[\frac{U_{N-1}}{\sigma_{N-1}} [f(z_N, t_N) - f(\mu_{N-1}, t_N)] \right]. \quad (24)$$

3.2 Main Theorem

The above discussion is summarized in the following theorem; see Appendix B for a detailed proof.

Theorem 3.1. *Let $\{z_n\}_{n=0}^{n_f}$ be the Markov process defined by the EM scheme (14) (15). Let N be a random variable uniformly distributed on $\{1, \dots, n_f\}$ and independent of z_0 and the U_n 's. Then the cross-entropy term in VAE training*

loss can be rewritten as:

$$\begin{aligned} \text{CE}(q_\phi(z_0|x)||p_\theta(z_0)) &\approx H(q_\phi(z_{n_f})) + \frac{1}{2}\mathbb{E}_{N,z_N} [g^2(t_N)||s_\theta(z_N, t_N)||_2^2] \\ &\quad + \mathbb{E}_{N,z_{N-1},z_N} \left[g^2(t_N) \frac{U_{N-1}}{\sigma_{N-1}} [s_\theta(z_N, t_N) - s_\theta(\mu_{N-1}, t_N)] \right] \\ &\quad - \mathbb{E}_{N,z_{N-1},z_N} \left[\frac{U_{N-1}}{\sigma_{N-1}} [f(z_N, t_N) - f(\mu_{N-1}, t_N)] \right]. \end{aligned} \quad (25)$$

Substituting (25) into the variational autoencoder loss (12) yields the final training objective. The encoder $q_\phi(z_0|x)$, the decoder $p_\psi(x|z_0)$, and the score network $s_\theta(z_t, t)$ are trained jointly by minimizing this final loss. We refer to the resulting latent SGM with a nonlinear noising process as LNDSM-SGM.

4 Experiments

Similar to [2], we demonstrate the enhanced performance of our proposed LNDSM-SGM in learning high-dimensional structured distributions using the MNIST dataset [14]. This dataset is a collection of 60,000 handwritten digits from 0 to 9, stored as 28×28 grayscale images (figure 1a). It exhibits a multimodal structure, in both the original space and, perhaps even more prominently, in a latent space, as each digit naturally forms at least one mode. For this reason, the reference distribution is chosen as a Gaussian mixture model (GMM) with 10 Gaussian components, where each component corresponds to the mode associated with one digit. We also consider a low-data regime, in which only 3,000 samples from the target distribution are used for training.

We further conduct experiments on the Approx.-C2-MNIST dataset. This dataset is constructed by randomly rotating each digit by 180° with probability 0.5, followed by resizing the rotated digits to half of their original size. As a result, the large digits remain upright, while the small digits appear upside down (Figure 3a). The dataset is referred to as Approx.-C2 because the samples can be viewed as drawn from a distribution that is approximately invariant under the discrete rotation group C_2 . The reference distribution in this case is a GMM with two Gaussian components: one corresponding to the large, upright digits, and the other to the small, upside-down digits.

The quality and variability of the generated samples are evaluated using the inception score [21] (IS, higher is better). The discrepancy between the generated distribution and the true distribution is quantified using the Fréchet inception distance [9] (FID, lower is better). To compute the FID, a ResNet-18 classifier is trained separately on the MNIST and Approx.-C2-MNIST datasets.

4.1 Implementation Details

Both the benchmark LSGM and our proposed LNDSM-SGM use the NVAE [23] architecture as the backbone of the VAE and the NCSNpp [22] as the backbone of the score network. By maintaining the identical network architectures, we ensure that any observed performance differences are attributable solely to the proposed LNDSM training objective. For the MNIST dataset, we simplify the NVAE architecture used in [24] by reducing the number of channels in both the feature maps and the latent variables; see Appendix C for details of the simplification and the NVAE building blocks. The dimension of the latent variables determined by the NVAE encoder is $2 \times 8 \times 8 = 128$. The NCSNpp-based score network is also simplified from the version used in [24]: the number of base channels is reduced from 256 to 32, the number of residual blocks in U-net downsampling path is reduced from 16 to 4, and the number of residual blocks in the upsampling path is reduced from 18 to 6. The numbers of trainable parameters for all networks are reported in Table 1. We also include the score network used in [2], which is based on a U-net [20]. The simplifications to NVAE and NCSNpp are designed to ensure that their combined number of trainable parameters is comparable to that of the U-net.

Table 1: Number of trainable parameters

Networks	# trainable parameters
NVAE	207,648
NCSNpp	895,076
NVAE + NCSNpp	1,102,724
U-Net in NDSM-SGM	1,115,297

For the benchmark LSGM, we adopt the Variance-Preserving (VP) SDE [22] as the forward diffusion process in the latent space:

$$dz_t = -\frac{1}{2}\beta(t)z_t dt + \sqrt{\beta(t)}dw_t, \quad (26)$$

where $\beta(t)$ is a linear function on $[0, T]$ with $\beta(0) = 0.1$ and $\beta(T) = 20$. The terminal time T is chosen to be 1. Following [24], the VAE is pretrained for 200 epochs and used to initialize the VAE in the benchmark LSGM. The VAE and the score network are then trained jointly using the Adam optimizer [12] with a batch size of 120 on a V-100-32GB GPU. The learning rates are 10^{-4} and 3×10^{-4} respectively. The number of training epochs is 500 for the full-data regime (both MNIST and Approx.-C2-MNIST) and 1000 for the low-data regime.

For our proposed LNDSM-SGM, the VAE encoder maps the training samples to the latent space, where a GMM reference distribution is fitted using the latent variables. The VAE is initialized to be the VAE trained under the benchmark LSGM for 100 epochs, and its learning rate is set to 10^{-6} , which is much smaller than 10^{-4} . Since the entropy of the GMM reference distribution in the training loss has no closed-form expression, this initialization together with the small learning rate ensures that the latent variables remain sufficiently expressive and do not change significantly during training. Therefore, the fitted GMM in the latent space can be regarded as approximately fixed, and its entropy term is removed from the training loss. The terminal time of the latent space forward diffusion process 1 is set to $T = 1.5$, and the number of time steps in the EM scheme is set to 100. The VAE and the score network are trained jointly using the Adam optimizer with a batch size of 60 on a V-100-32GB GPU for 50 epochs for both regimes.

4.2 Results Comparison

An import technical component of the benchmark LSGM is importance sampling (Appendix B in [24]). The expectation \mathbb{E}_t in (5) has high variance if t is uniformly sampled from $[0, T]$, which leads to ineffective training and poor sample quality, as reflected by large FID values. Importance sampling alleviates this issue by drawing t from a suitably designed importance distribution. Although this approach is empirically effective, its derivation relies on the assumption that the latent target distribution is standard Gaussian. In contrast, for the proposed LNDSM-SGM, all trajectories generated by the EM scheme are directly used to compute the training loss (25). As a result, no additional importance sampling is required for variance reduction.

A limitation of NDSM-SGM [2] is its slow synthesis speed, which is dominated by the cost of simulating the forward SDE via the EM method. In (6), the state variables are 784-dimensional vectors, and the EM discretization uses 1000 steps. With a batch size of 60, the average simulation time is 0.35 seconds. Our proposed LNDSM-SGM achieves substantially faster synthesis. Variables in the SDE (11) are 128-dimensional vectors in the latent space. Because of the joint training setup, gradients of these variables w.r.t the parameters of the VAE are stored. The latent representations allow for smaller number of EM discretization steps, which is 100. This choice is justified by the empirical fact that the probability flow ODE is usually much less complex in the latent space [24]. The resulting average simulation time is 0.068 seconds with a batch size of 60.

Because of the EM scheme, each training epoch of LNDSM-SGM is computationally more expensive, requiring on average 600 seconds per epoch, compared with 80 seconds per epoch for the benchmark LSGM. However, the latent variables generated by the EM scheme are directly used to evaluate the training loss (25) and are therefore not wasted. Moreover, LNDSM-SGM only needs 50 training epochs to convergence, whereas the benchmark LSGM requires 500 epochs in the full-data regime and 1000 epochs in the low-data regime. Consequently, the total training time of the proposed LNDSM-SGM is lower.

After training, 10,000 samples are generated by simulating the reverse-time SDE or the corresponding probability flow ODE [22], with the marginal score replaced by the trained score network. These samples are used to compute the FID and IS. A snapshot (64 out of 10,000 samples) and the empirical fraction of different digits are visualized in Figures 1, 2, and 3. The same evaluation pipeline is applied to both the benchmark LSGM and the proposed LNDSM-SGM.

The samples generated by the benchmark LSGM exhibit mode imbalance (Figure 1e, 2e, and 3e). The empirical fractions of generated digits differ significantly from the target fractions in the training data (Figures 1d, 2d, and 3d). This imbalance is largely resolved by the proposed LNDSM-SGM. By introducing a GMM reference distribution to impose the multimodal structure, the fractions of generated digits closely match the target distribution, especially for the MNIST and the Approx.-C2-MNIST (Figure 1f and 3f). In the low-data MNIST setting, although some discrepancy remains (Figure 2f), LNDSM-SGM captures the relative magnitude of digit frequencies more accurately than the benchmark LSGM.

The best FID values and the corresponding IS achieved during the training process are reported in Tables 2 and 3. The exhibited FID and IS for NDSM-SGM on MNIST are taken from [2]. The benchmark LSGM outperforms

the NDSM-SGM in both FID and IS, which can be attributed to the mapping of high-dimensional data into a more compact and informative latent space that facilitates density estimation. The proposed LNDSM-SGM further improves upon LSGM, achieving substantially lower FID and higher IS on both MNIST and low-data MNIST. These results demonstrate the enhanced capability of LNDSM-SGM in learning structured target distributions.

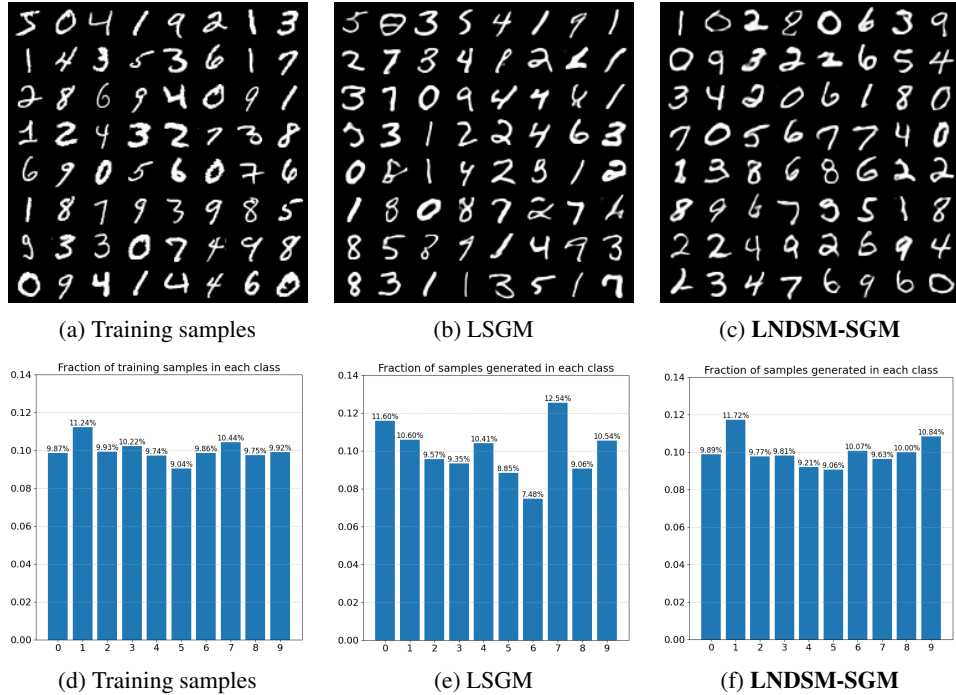


Figure 1: LSGM and LNDSM-SGM trained using the full MNIST dataset. (a) and (d): Snapshot and fraction of different digits of the training samples. (b) and (e): Snapshot and fraction of different digits of the 10,000 samples generated by the LSGM. The KL divergence from the fraction of the training samples to the fraction of the generated samples: 0.008. (c) and (f): Snapshot and fraction of different digits of the 10,000 samples generated by the LNDSM-SGM. The KL divergence from the fraction of the training samples to the fraction of the generated samples: 0.00114.

Table 2: FID and IS on MNIST

model	FID (\downarrow)	IS (\uparrow)
NDSM-SGM	36.1	8.93
LSGM	6.7	9.42
LNDSM-SGM	2.2	9.75

5 Conclusion

We presented latent nonlinear denoising score matching (LNDSM), which integrates nonlinear diffusions and structured latent priors into the latent score-based generative modeling framework. By reformulating the VAE-induced cross-entropy via an Euler–Maruyama discretization and conditional Gaussian transitions, and by removing two variance-exploding control variates, LNDSM yields a numerically stable training objective that does not require importance sampling in time. Using Gaussian mixture models as latent reference distributions, LNDSM-SGM effectively encodes multimodal and approximately symmetric structure in the latent space. Experiments on MNIST and Approx.-C2-MNIST, including low-data regimes, show that LNDSM-SGM achieves substantially lower Fréchet inception distance, higher inception score, improved mode balance, and reduced overall training time compared to LSGM and NDSM-SGM, indicating that nonlinear latent diffusions with structured latent priors provide an efficient and powerful approach for learning structured data distributions.

Acknowledgments

This material is based upon work supported by the U.S. National Science Foundation under the award DMS-2502900 and by the Air Force Office of Scientific Research (AFOSR) under Grant No. FA9550-25-1-0079.

References

- [1] Brian D. O. Anderson. Reverse-time diffusion equation models. *Stochastic Processes and their Applications*, 12(3):313–326, 1982.
- [2] Jeremiah Birrell, Markos A. Katsoulakis, Luc Rey-Bellet, Benjamin J. Zhang, and Wei Zhu. Nonlinear denoising score matching for enhanced learning of structured distributions. *Computer Methods in Applied Mechanics and Engineering*, 446:118226, 2025.
- [3] Jeremiah Birrell, Markos A. Katsoulakis, Luc Rey-Bellet, and Wei Zhu. Structure-preserving gans, 2022.
- [4] Andreas Blattmann, Robin Rombach, Huan Ling, Tim Dockhorn, Seung Wook Kim, Sanja Fidler, and Karsten Kreis. Align your latents: High-resolution video synthesis with latent diffusion models. In *Proceedings of the IEEE/CVF conference on computer vision and pattern recognition*, pages 22563–22575, 2023.
- [5] Djork-Arné Clevert, Thomas Unterthiner, and Sepp Hochreiter. Fast and accurate deep network learning by exponential linear units (elus), 2016.
- [6] Neel Dey, Antong Chen, and Soheil Ghafurian. Group equivariant generative adversarial networks. In *International Conference on Learning Representations*.
- [7] Prafulla Dhariwal and Alex Nichol. Diffusion models beat gans on image synthesis. *CoRR*, abs/2105.05233, 2021.
- [8] Ian J. Goodfellow, Jean Pouget-Abadie, Mehdi Mirza, Bing Xu, David Warde-Farley, Sherjil Ozair, Aaron Courville, and Yoshua Bengio. Generative adversarial networks, 2014.
- [9] Martin Heusel, Hubert Ramsauer, Thomas Unterthiner, Bernhard Nessler, and Sepp Hochreiter. Gans trained by a two time-scale update rule converge to a local nash equilibrium. In *Proceedings of the 31st International Conference on Neural Information Processing Systems, NIPS’17*, page 6629–6640, Red Hook, NY, USA, 2017. Curran Associates Inc.
- [10] Jonathan Ho, Ajay Jain, and Pieter Abbeel. Denoising diffusion probabilistic models, 2020.
- [11] Jie Hu, Li Shen, Samuel Albanie, Gang Sun, and Enhua Wu. Squeeze-and-excitation networks, 2019.
- [12] Diederik P. Kingma and Jimmy Ba. Adam: A method for stochastic optimization. *International Conference on Learning Representations (ICLR)*, 2015.
- [13] Diederik P Kingma and Max Welling. Auto-encoding variational bayes, 2022.
- [14] Y. Lecun, L. Bottou, Y. Bengio, and P. Haffner. Gradient-based learning applied to document recognition. *Proceedings of the IEEE*, 86(11):2278–2324, 1998.
- [15] Yaron Lipman, Ricky T. Q. Chen, Heli Ben-Hamu, Maximilian Nickel, and Matt Le. Flow matching for generative modeling, 2023.
- [16] Haoye Lu, Spencer Szabados, and Yaoliang Yu. Diffusion models under group transformations. In Yingzhen Li, Stephan Mandt, Shipra Agrawal, and Emtiyaz Khan, editors, *Proceedings of The 28th International Conference on Artificial Intelligence and Statistics*, volume 258 of *Proceedings of Machine Learning Research*, pages 3538–3546. PMLR, 03–05 May 2025.
- [17] Walter HL Pinaya, Petru-Daniel Tudosiu, Jessica Dafflon, Pedro F Da Costa, Virginia Fernandez, Parashkev Nachev, Sebastien Ourselin, and M Jorge Cardoso. Brain imaging generation with latent diffusion models. In *MICCAI workshop on deep generative models*, pages 117–126. Springer, 2022.
- [18] Prajit Ramachandran, Barret Zoph, and Quoc V. Le. Searching for activation functions, 2017.
- [19] Robin Rombach, Andreas Blattmann, Dominik Lorenz, Patrick Esser, and Björn Ommer. High-resolution image synthesis with latent diffusion models, 2022.
- [20] Olaf Ronneberger, Philipp Fischer, and Thomas Brox. U-net: Convolutional networks for biomedical image segmentation, 2015.
- [21] Tim Salimans, Ian Goodfellow, Wojciech Zaremba, Vicki Cheung, Alec Radford, and Xi Chen. Improved techniques for training gans. In *Proceedings of the 30th International Conference on Neural Information Processing Systems, NIPS’16*, page 2234–2242, Red Hook, NY, USA, 2016. Curran Associates Inc.
- [22] Yang Song, Jascha Sohl-Dickstein, Diederik P Kingma, Abhishek Kumar, Stefano Ermon, and Ben Poole. Score-based generative modeling through stochastic differential equations. In *International Conference on Learning Representations*, 2021.
- [23] Arash Vahdat and Jan Kautz. Nvae: a deep hierarchical variational autoencoder. In *Proceedings of the 34th International Conference on Neural Information Processing Systems, NIPS ’20*, Red Hook, NY, USA, 2020. Curran Associates Inc.

-
- [24] Arash Vahdat, Karsten Kreis, and Jan Kautz. Score-based generative modeling in latent space. In *Proceedings of the 35th International Conference on Neural Information Processing Systems*, NIPS '21, Red Hook, NY, USA, 2021. Curran Associates Inc.
 - [25] Pascal Vincent. A connection between score matching and denoising autoencoders. *Neural Computation*, 23(7):1661–1674, 2011.
 - [26] Minkai Xu, Alexander S Powers, Ron O Dror, Stefano Ermon, and Jure Leskovec. Geometric latent diffusion models for 3d molecule generation. In *International Conference on Machine Learning*, pages 38592–38610. PMLR, 2023.

A Lemma about Cross Entropy

The following lemma is an extension of the theorem in Appendix A of [24] to a generic diffusion process. Specifically, the time interval is extended from $[0, 1]$ to $[0, T]$. Accordingly, the proof follows the same structure as in [24], prior to the specialization to a linear drift coefficient. For completeness, we provide full derivations and expand the steps that were abbreviated in the original proof.

Lemma 1. *Let $q(z_0)$ and $p(z_0)$ be the densities of two distributions defined in the latent space. Consider the generic diffusion process*

$$dz_t = f(z_t, t)dt + g(t)dw_t, \quad (27)$$

where the drift $f(z_t, t)$ is not necessarily linear in z_t . Denote the corresponding marginal densities at time $t \in [0, T]$ by $q(z_t)$ and $p(z_t)$. Assume that $q(z_T) = p(z_T)$, and that $\log q(z_t)$ and $\log p(z_t)$ are smooth functions with at most polynomial growth as $z_t \rightarrow \pm\infty$. Then the cross entropy $\text{CE}(q(z_0)||p(z_0))$ between $q(z_0)$ and $p(z_0)$ satisfies

$$\begin{aligned} \text{CE}(q(z_0)||p(z_0)) &= H(q(z_T)) + \int_0^T \mathbb{E}_{q(z_t)} \left[\frac{1}{2} g^2(t) \|\nabla_{z_t} \log p(z_t)\|_2^2 + f^T(z_t, t) \nabla_{z_t} \log q(z_t) \right. \\ &\quad \left. - g^2(t) [\nabla_{z_t} \log q(z_t)]^T \nabla_{z_t} \log p(z_t) \right] dt. \end{aligned}$$

Proof. The densities $q(z_t)$ and $p(z_t)$ satisfy the Fokker-Planck equations

$$\frac{\partial q(z_t)}{\partial t} = \nabla_{z_t} \left[\frac{1}{2} g^2(t) q(z_t) \nabla_{z_t} \log q(z_t) - f(z_t, t) q(z_t) \right] := \nabla_{z_t} [h_q(z_t, t) q(z_t)], \quad (28)$$

$$\frac{\partial p(z_t)}{\partial t} = \nabla_{z_t} \left[\frac{1}{2} g^2(t) p(z_t) \nabla_{z_t} \log p(z_t) - f(z_t, t) p(z_t) \right] := \nabla_{z_t} [h_p(z_t, t) p(z_t)]. \quad (29)$$

Rewrite the cross entropy $\text{CE}(q(z_0)||p(z_0))$ by adding and subtracting an extra term:

$$\begin{aligned} \text{CE}(q(z_0)||p(z_0)) &= \text{CE}(q(z_T)||p(z_T)) - \text{CE}(q(z_T)||p(z_T)) + \text{CE}(q(z_0)||p(z_0)) \\ &= \text{CE}(q(z_T)||p(z_T)) - \int_0^T \frac{\partial}{\partial t} \text{CE}(q(z_t)||p(z_t)) dt \\ &= H(q(z_T)) - \int_0^T \frac{\partial}{\partial t} \text{CE}(q(z_t)||p(z_t)) dt. \end{aligned} \quad (30)$$

The third equality uses the assumption $q(z_T) = p(z_T)$, and $H(q(z_T))$ is the entropy of $q(z_T)$.

Next, for the time derivative $\frac{\partial}{\partial t} \text{CE}(q(z_t)||p(z_t))$ in (30):

$$\begin{aligned} \frac{\partial}{\partial t} \text{CE}(q(z_t)||p(z_t)) &= \frac{\partial}{\partial t} \int -q(z_t) \log p(z_t) dz_t \\ &= - \int \left[\frac{\partial q(z_t)}{\partial t} \log p(z_t) + \frac{q(z_t)}{p(z_t)} \frac{\partial p(z_t)}{\partial t} \right] dz_t \\ &= - \int \left[\nabla_{z_t} [h_q(z_t, t) q(z_t)] \log p(z_t) + \frac{q(z_t)}{p(z_t)} \nabla_{z_t} [h_p(z_t, t) p(z_t)] \right] dz_t. \end{aligned} \quad (31)$$

The third equality is due to the Fokker-Planck equations (28) and (29).

Since $q(z_t)$ and $p(z_t)$ are probability densities, they are normalized and therefore satisfy $q(z_t), p(z_t) \rightarrow 0$ as $z_t \rightarrow \pm\infty$. By assumption, $\log q(z_t)$ and $\log p(z_t)$ are smooth functions with at most polynomial growth as $z_t \rightarrow \pm\infty$. Consequently, their gradients $\nabla_{z_t} \log q(z_t)$ and $\nabla_{z_t} \log p(z_t)$ are also smooth and exhibit at most polynomial growth. Moreover, $q(z_t)$ and $p(z_t)$ decay at least exponentially fast. Therefore, the following limits hold:

$$\log p(z_t) h_q(z_t, t) q(z_t) = \log p(z_t) \left[\frac{1}{2} g^2(t) \nabla_{z_t} \log q(z_t) - f(z_t, t) \right] q(z_t) \rightarrow 0, z_t \rightarrow \pm\infty, \quad (32)$$

$$\log q(z_t) h_p(z_t, t) p(z_t) = \log q(z_t) \left[\frac{1}{2} g^2(t) \nabla_{z_t} \log p(z_t) - f(z_t, t) \right] p(z_t) \rightarrow 0, z_t \rightarrow \pm\infty. \quad (33)$$

Applying integration by parts yields

$$\begin{aligned}
& \int \nabla_{z_t} [h_q(z_t, t) q(z_t)] \log p(z_t) dz_t = \int \log p(z_t) d[h_q(z_t, t) q(z_t)] \\
& = \log p(z_t) h_q(z_t, t) q(z_t) \big|_{z_t \rightarrow \pm \infty} - \int [h_q(z_t, t)]^T q(z_t) \nabla_{z_t} \log p(z_t) dz_t \\
& = - \int [h_q(z_t, t)]^T q(z_t) \nabla_{z_t} \log p(z_t) dz_t.
\end{aligned} \tag{34}$$

Similarly,

$$\begin{aligned}
& \int \frac{q(z_t)}{p(z_t)} \nabla_{z_t} [h_p(z_t, t) p(z_t)] dz_t = \int \frac{q(z_t)}{p(z_t)} d[h_p(z_t, t) p(z_t)] \\
& = \frac{q(z_t)}{p(z_t)} h_p(z_t, t) p(z_t) \big|_{z_t \rightarrow \pm \infty} - \int [h_p(z_t, t)]^T p(z_t) \nabla_{z_t} \frac{q(z_t)}{p(z_t)} dz_t \\
& = - \int [h_p(z_t, t)]^T p(z_t) \nabla_{z_t} \frac{q(z_t)}{p(z_t)} dz_t.
\end{aligned} \tag{35}$$

Substituting these into (31) gives

$$\frac{\partial}{\partial t} \text{CE}(q(z_t) \| p(z_t)) = \int [h_q(z_t, t)]^T q(z_t) \nabla_{z_t} \log p(z_t) dz_t + \int [h_p(z_t, t)]^T p(z_t) \nabla_{z_t} \frac{q(z_t)}{p(z_t)} dz_t. \tag{36}$$

Using the log-derivative identity, we obtain

$$\begin{aligned}
& \int [h_p(z_t, t)]^T p(z_t) \nabla_{z_t} \frac{q(z_t)}{p(z_t)} dz_t \\
& = \int [h_p(z_t, t)]^T q(z_t) \frac{p(z_t)}{q(z_t)} \nabla_{z_t} \frac{q(z_t)}{p(z_t)} dz_t = \int [h_p(z_t, t)]^T q(z_t) \nabla_{z_t} \log \frac{q(z_t)}{p(z_t)} dz_t \\
& = \int [h_p(z_t, t)]^T q(z_t) \nabla_{z_t} \log q(z_t) dz_t - \int [h_p(z_t, t)]^T q(z_t) \nabla_{z_t} \log p(z_t) dz_t.
\end{aligned} \tag{37}$$

Apply (37) and expressions of $h_p(z_t, t)$ and $h_q(z_t, t)$ to (36):

$$\begin{aligned}
& \frac{\partial}{\partial t} \text{CE}(q(z_t) \| p(z_t)) \\
& = \int q(z_t) \{ [h_q(z_t, t)]^T \nabla_{z_t} \log p(z_t) + [h_p(z_t, t)]^T \nabla_{z_t} \log q(z_t) - [h_p(z_t, t)]^T \nabla_{z_t} \log p(z_t) \} dz_t \\
& = \int q(z_t) \left\{ \frac{1}{2} g^2(t) [\nabla_{z_t} \log q(z_t)]^T \nabla_{z_t} \log p(z_t) - f^T(z_t, t) \nabla_{z_t} \log p(z_t) \right. \\
& \quad + \frac{1}{2} g^2(t) [\nabla_{z_t} \log p(z_t)]^T \nabla_{z_t} \log q(z_t) - f^T(z_t, t) \nabla_{z_t} \log q(z_t) \\
& \quad \left. - \frac{1}{2} g^2(t) [\nabla_{z_t} \log p(z_t)]^T \nabla_{z_t} \log p(z_t) + f^T(z_t, t) \nabla_{z_t} \log p(z_t) \right\} dz_t \\
& = \int q(z_t) \left[-\frac{1}{2} g^2(t) \|\nabla_{z_t} \log p(z_t)\|_2^2 - f^T(z_t, t) \nabla_{z_t} \log q(z_t) + g^2(t) [\nabla_{z_t} \log q(z_t)]^T \nabla_{z_t} \log p(z_t) \right] dz_t.
\end{aligned} \tag{38}$$

Finally, substituting (38) into (30) proves the result:

$$\begin{aligned}
& \text{CE}(q(z_0) \| p(z_0)) \\
& = H(q(z_T)) - \int_0^T \frac{\partial}{\partial t} \text{CE}(q(z_t) \| p(z_t)) dt \\
& = H(q(z_T)) + \int_0^T \mathbb{E}_{q(z_t)} \left[\frac{1}{2} g^2(t) \|\nabla_{z_t} \log p(z_t)\|_2^2 + f^T(z_t, t) \nabla_{z_t} \log q(z_t) - g^2(t) [\nabla_{z_t} \log q(z_t)]^T \nabla_{z_t} \log p(z_t) \right] dt.
\end{aligned} \tag{39}$$

□

B Proof of Theorem 3.1

Theorem 3.1. Let $\{z_n\}_{n=0}^{n_f}$ be the Markov process defined by the EM scheme (14) (15). Let N be a random variable uniformly distributed on $\{1, \dots, n_f\}$ and independent of z_0 and the U_n 's. Then the cross-entropy term in VAE training loss can be rewritten as:

$$\begin{aligned} \text{CE}(q_\phi(z_0|x)||p_\theta(z_0)) &\approx H(q_\phi(z_{n_f})) + \frac{1}{2}\mathbb{E}_{N,z_N} [g^2(t_N)||s_\theta(z_N, t_N)||_2^2] \\ &\quad + \mathbb{E}_{N,z_{N-1},z_N} \left[g^2(t_N) \frac{U_{N-1}}{\sigma_{N-1}} [s_\theta(z_N, t_N) - s_\theta(\mu_{N-1}, t_N)] \right] \\ &\quad - \mathbb{E}_{N,z_{N-1},z_N} \left[\frac{U_{N-1}}{\sigma_{N-1}} [f(z_N, t_N) - f(\mu_{N-1}, t_N)] \right]. \end{aligned} \quad (40)$$

Proof. View the densities $q_\phi(z_0|x)$ and $p_\theta(z_0)$ as $q(z_0)$ and $p(z_0)$ in Lemma 1. By adding and subtracting the term $\frac{1}{2}g^2(t)\|\nabla_{z_t} \log q_\phi(z_t|x)\|_2^2$, the cross-entropy term in the loss (12) can be written as

$$\begin{aligned} &\text{CE}(q_\phi(z_0|x)||p_\theta(z_0)) \\ &= H(q_\phi(z_T|x)) \\ &\quad + \int_0^T \mathbb{E}_{q_\phi(z_t|x)} \left[\frac{1}{2}g^2(t)\|\nabla_{z_t} \log p_\theta(z_t)\|_2^2 + f^T(z_t, t)\nabla_{z_t} \log q_\phi(z_t|x) - g^2(t) [\nabla_{z_t} \log q_\phi(z_t|x)]^T \nabla_{z_t} \log p_\theta(z_t) \right] dt \\ &= H(q_\phi(z_T|x)) \\ &\quad + \frac{1}{2} \int_0^T g^2(t) \mathbb{E}_{q_\phi(z_t|x)} [\|\nabla_{z_t} \log q_\phi(z_t|x) - \nabla_{z_t} \log p_\theta(z_t)\|_2^2] dt \\ &\quad + \frac{1}{2} \int_0^T \mathbb{E}_{q_\phi(z_t|x)} \left[[2f(z_t, t) - g^2(t)\nabla_{z_t} \log q_\phi(z_t|x)]^T \nabla_{z_t} \log q_\phi(z_t|x) \right] dt \\ &= H(q_\phi(z_T|x)) \\ &\quad + \frac{1}{2} \int_0^T g^2(t) \mathbb{E}_{q_\phi(z_t|x)} [\|\nabla_{z_t} \log q_\phi(z_t|x) - s_\theta(z_t, t)\|_2^2] dt \\ &\quad + \frac{1}{2} \int_0^T \mathbb{E}_{q_\phi(z_t|x)} \left[[2f(z_t, t) - g^2(t)\nabla_{z_t} \log q_\phi(z_t|x)]^T \nabla_{z_t} \log q_\phi(z_t|x) \right] dt. \end{aligned} \quad (41)$$

The second equality follows from completing the square after adding and subtracting the extra term. Here $\nabla_{z_t} \log p_\theta(z_t)$ is the score of the marginal distribution at time t , which is parameterized by the score network $s_\theta(z_t, t)$. Combined with the Markov process (14) (15), the cross entropy (41) can be approximated by:

$$\begin{aligned} &\text{CE}(q_\phi(z_0|x)||p_\theta(z_0)) \\ &\approx H(q_\phi(z_{n_f})) \\ &\quad + \frac{1}{2}\mathbb{E}_{N,z_N} [g^2(t_N)||\nabla_{z_N} \log q_\phi(z_N) - s_\theta(z_N, t_N)||_2^2] \\ &\quad + \frac{1}{2}\mathbb{E}_{N,z_N} \left[[2f(z_N, t_N) - g^2(t_N)\nabla_{z_N} \log q_\phi(z_N)]^T \nabla_{z_N} \log q_\phi(z_N) \right]. \end{aligned} \quad (42)$$

Here, the continuous time variable t is replaced by the discrete time steps t_N , and the latent variable z_t is replaced by z_N in the discrete Markov process. Split the second squared norm term in (42), also consider N takes some value n for simplicity:

$$\begin{aligned} &\frac{1}{2}\mathbb{E}_{z_n} [g^2(t_n)||\nabla_{z_n} \log q_\phi(z_n) - s_\theta(z_n, t_n)||_2^2] \\ &= \frac{1}{2}\mathbb{E}_{z_n} [g^2(t_n)||s_\theta(z_n, t_n)||_2^2] - \mathbb{E}_{z_n} [g^2(t_n)s_\theta(z_n, t_n) \cdot \nabla_{z_n} \log q_\phi(z_n)] + \frac{1}{2}\mathbb{E}_{z_n} [g^2(t_n)||\nabla_{z_n} \log q_\phi(z_n)||_2^2]. \end{aligned} \quad (43)$$

The second inner product term in (43) can be written in integral as

$$\begin{aligned}
& \mathbb{E}_{z_n} [g^2(t_n) s_\theta(z_n, t_n) \cdot \nabla_{z_n} \log q_\phi(z_n)] \\
&= g^2(t_n) \int s_\theta(z_n, t_n) \cdot q_\phi(z_n) \nabla_{z_n} \log q_\phi(z_n) dz_n \\
&= g^2(t_n) \int s_\theta(z_n, t_n) \cdot \nabla_{z_n} q_\phi(z_n) dz_n \\
&= g^2(t_n) \int s_\theta(z_n, t_n) \cdot \nabla_{z_n} \left[\int \cdots \int q_\phi(z_n | z_{n-1}) \cdots q_\phi(z_1 | z_0) q_\phi(z_0) dz_0 dz_1 \cdots dz_{n-1} \right] dz_n \\
&= g^2(t_n) \int \cdots \int \int [s_\theta(z_n, t_n) \cdot \nabla_{z_n} \log q_\phi(z_n | z_{n-1})] q_\phi(z_n | z_{n-1}) \cdots q_\phi(z_1 | z_0) q_\phi(z_0) dz_0 dz_1 \cdots dz_{n-1} dz_n
\end{aligned} \tag{44}$$

The second and fourth equality use the identity $x d \log x = x \frac{d \log x}{dx} dx = dx$. Since z_0, \dots, z_n form a Markov chain, they satisfy

$$q_\phi(z_n | z_{n-1}) \cdots q_\phi(z_1 | z_0) q_\phi(z_0) = q_\phi(z_n, z_{n-1}, \dots, z_1, z_0). \tag{45}$$

Substituting (45) into (44) yields

$$\begin{aligned}
& \mathbb{E}_{z_n} [g^2(t_n) s_\theta(z_n, t_n) \cdot \nabla_{z_n} \log q_\phi(z_n)] \\
&= g^2(t_n) \int \int s_\theta(z_n, t_n) \cdot \nabla_{z_n} \log q_\phi(z_n | z_{n-1}) \left[\int \int q_\phi(z_n, z_{n-1}, \dots, z_1, z_0) dz_0 dz_1 \cdots dz_{n-2} \right] dz_{n-1} dz_n.
\end{aligned} \tag{46}$$

The inner product $s_\theta(z_n, n) \cdot \nabla_{z_n} \log q_\phi(z_n | z_{n-1})$ depends only on z_n, z_{n-1} , and the inner integral gives the joint density of (z_n, z_{n-1}) . Thus the integral in (44) can be rewritten as

$$\mathbb{E}_{z_n} [g^2(t_n) s_\theta(z_n, t_n) \cdot \nabla_{z_n} \log q_\phi(z_n)] = g^2(t_n) \mathbb{E}_{z_{n-1}, z_n} [s_\theta(z_n, t_n) \cdot \nabla_{z_n} \log q_\phi(z_n | z_{n-1})]. \tag{47}$$

Since $z_n = \mu_{n-1} + \sigma_{n-1} U_{n-1}$, which is approximately Gaussian when Δt_{n-1} is small enough, the score of the transitional distribution $q_\phi(z_n | z_{n-1})$ has closed form:

$$\nabla_{z_n} \log q_\phi(z_n | z_{n-1}) = -\frac{U_{n-1}}{\sigma_{n-1}}. \tag{48}$$

Then the rewritten integral (47) becomes:

$$\mathbb{E}_{z_n} [g^2(t_n) s_\theta(z_n, t_n) \cdot \nabla_{z_n} \log q_\phi(z_n)] = -g^2(t_n) \mathbb{E}_{z_{n-1}, z_n} \left[s_\theta(z_n, t_n) \cdot \frac{U_{n-1}}{\sigma_{n-1}} \right]. \tag{49}$$

Note that $\sigma_{n-1} = g(t_{n-1}) \sqrt{\Delta t_{n-1}}$ (15), where g is the diffusion coefficient of the diffusion process determined by the reference distribution. When Δt_{n-1} is very small, $\frac{1}{\sigma_{n-1}}$ becomes large, leading to high variance. On the other hand, in order for $q_\phi(z_n | z_{n-1})$ to be well approximated by a Gaussian, the EM discretization must be fine, so Δt_{n-1} must indeed be small. To address this issue, consider the Taylor expansion of the score network:

$$\begin{aligned}
s_\theta(z_n, t_n) &= s_\theta(\mu_{n-1} + \sigma_{n-1} U_{n-1}, t_n) \\
&= s_\theta(\mu_{n-1}, t_n) + \nabla_{\mu_{n-1}} s_\theta(\mu_{n-1}, t_n) \cdot \sigma_{n-1} U_{n-1} + O(\sigma_{n-1}^2).
\end{aligned} \tag{50}$$

Multiplying both sides of (50) by $\frac{U_{n-1}}{\sigma_{n-1}}$ gives

$$s_\theta(z_n, t_n) \cdot \frac{U_{n-1}}{\sigma_{n-1}} = s_\theta(\mu_{n-1}, t_n) \cdot \frac{U_{n-1}}{\sigma_{n-1}} + [\nabla_{\mu_{n-1}} s_\theta(\mu_{n-1}, t_n) \cdot U_{n-1}] U_{n-1} + O(\sigma_{n-1}). \tag{51}$$

The first term on the right-hand side, $s_\theta(\mu_{n-1}, t_n) \cdot \frac{U_{n-1}}{\sigma_{n-1}}$, becomes large when σ_{n-1} is small, but has zero expectation since $U_{n-1} \sim \mathcal{N}(0, I)$. Hence it can be subtracted as a control variate:

$$\begin{aligned}
& \mathbb{E}_{z_{n-1}, z_n} \left[s_\theta(\mu_{n-1}, t_n) \cdot \frac{U_{n-1}}{\sigma_{n-1}} \right] = \mathbb{E}_{z_{n-1}} \left[\frac{s_\theta(\mu_{n-1}, t_n)}{\sigma_{n-1}} \mathbb{E}_{z_n} [U_{n-1}] \right] = 0 \\
& \Rightarrow \mathbb{E}_{z_{n-1}, z_n} \left[s_\theta(z_n, t_n) \cdot \frac{U_{n-1}}{\sigma_{n-1}} \right] \\
& = \mathbb{E}_{z_{n-1}, z_n} \left[s_\theta(z_n, t_n) \cdot \frac{U_{n-1}}{\sigma_{n-1}} - s_\theta(\mu_{n-1}, t_n) \cdot \frac{U_{n-1}}{\sigma_{n-1}} \right] \\
& = \mathbb{E}_{z_{n-1}, z_n} \left[\frac{U_{n-1}}{\sigma_{n-1}} \cdot [s_\theta(z_n, t_n) - s_\theta(\mu_{n-1}, t_n)] \right]. \tag{52}
\end{aligned}$$

Substituting (49) and (52) into (43) yields

$$\begin{aligned}
& \frac{1}{2} \mathbb{E}_{z_n} [g^2(t_n) \|\nabla_{z_n} \log q_\phi(z_n) - s_\theta(z_n, t_n)\|_2^2] \\
& = \frac{1}{2} \mathbb{E}_{z_n} [g^2(t_n) \|s_\theta(z_n, t_n)\|_2^2] \\
& \quad + g^2(t_n) \mathbb{E}_{z_{n-1}, z_n} \left[\frac{U_{n-1}}{\sigma_{n-1}} \cdot [s_\theta(z_n, t_n) - s_\theta(\mu_{n-1}, t_n)] \right] \\
& \quad + \frac{1}{2} \mathbb{E}_{z_n} [g^2(t_n) \|\nabla_{z_n} \log q_\phi(z_n)\|_2^2]. \tag{53}
\end{aligned}$$

For simplicity, the above discussion is based on N takes some value n . Reintroducing the random index N in place of n gives

$$\begin{aligned}
& \frac{1}{2} \mathbb{E}_{N, z_N} [g^2(t_N) \|\nabla_{z_N} \log q_\phi(z_N) - s_\theta(z_N, t_N)\|_2^2] \\
& = \frac{1}{2} \mathbb{E}_{N, z_N} [g^2(t_N) \|s_\theta(z_N, t_N)\|_2^2] \\
& \quad + \mathbb{E} \left[g^2(t_N) \mathbb{E}_{z_{N-1}, z_N} \left[\frac{U_{N-1}}{\sigma_{N-1}} \cdot [s_\theta(z_N, t_N) - s_\theta(\mu_{N-1}, t_N)] \right] \right] \\
& \quad + \frac{1}{2} \mathbb{E}_{N, z_N} [g^2(t_N) \|\nabla_{z_N} \log q_\phi(z_N)\|_2^2]. \tag{54}
\end{aligned}$$

The third squared norm term in (54) can be cancelled out by part of the third inner product term in (42). So now the cross entropy term in the loss function can be written as:

$$\begin{aligned}
& \text{CE}(q_\phi(z_0|x) \| p_\theta(z_0)) \\
& = H(q_\phi(z_{n_f})) \\
& \quad + \frac{1}{2} \mathbb{E}_{N, z_N} [g^2(t_N) \|s_\theta(z_N, t_N)\|_2^2] + \mathbb{E}_N \left[g^2(t_N) \mathbb{E}_{z_{N-1}, z_N} \left[\frac{U_{N-1}}{\sigma_{N-1}} \cdot [s_\theta(z_N, t_N) - s_\theta(\mu_{N-1}, t_N)] \right] \right] \\
& \quad + \mathbb{E}_{N, z_N} [f(z_N, t_N) \cdot \nabla_{z_N} \log q_\phi(z_N)]. \tag{55}
\end{aligned}$$

For the third inner product term in (55), we can also write it in the form of integral as (44) to utilize the approximately Gaussian transition distribution. Also consider N takes some value n for simplicity:

$$\begin{aligned}
& \mathbb{E}_{z_n} [f(z_n, t_n) \cdot \nabla_{z_n} \log q_\phi(z_n)] \\
& = \int f(z_n, t_n) \cdot q_\phi(z_n) \nabla_{z_n} \log q_\phi(z_n) dz_n \\
& = \int f(z_n, t_n) \cdot \nabla_{z_n} q_\phi(z_n) dz_n \\
& = \int f(z_n, t_n) \cdot \nabla_{z_n} \left[\int \cdots \int \int q_\phi(z_n | z_{n-1}) \cdots q_\phi(z_1 | z_0) q_\phi(z_0) dz_0 dz_1 \cdots dz_{n-1} \right] dz_n \\
& = \int \cdots \int \int \int [f(z_n, t_n) \cdot \nabla_{z_n} \log q_\phi(z_n | z_{n-1})] q_\phi(z_n | z_{n-1}) \cdots q_\phi(z_1 | z_0) q_\phi(z_0) dz_0 dz_1 \cdots dz_{n-1} dz_n. \tag{56}
\end{aligned}$$

Similar to (44), based on the Markov property (45), we interpret (56) as

$$\mathbb{E}_{z_n} [f(z_n, t_n) \cdot \nabla_{z_n} \log q_\phi(z_n)] = \mathbb{E}_{z_{n-1}, z_n} [f(z_n, t_n) \cdot \nabla_{z_n} \log q_\phi(z_n | z_{n-1})]. \quad (57)$$

Using again that $q_\phi(z_n | z_{n-1})$ is approximately Gaussian, we obtain

$$\mathbb{E}_{z_n} [f(z_n, t_n) \cdot \nabla_{z_n} \log q_\phi(z_n)] = -\mathbb{E}_{z_{n-1}, z_n} \left[f(z_n, t_n) \cdot \frac{U_{n-1}}{\sigma_{n-1}} \right]. \quad (58)$$

This term also suffers from high variance when Δt_{n-1} is small. As before, we consider the Taylor expansion

$$f(z_n, t_n) = f(\mu_{n-1}, t_n) + \nabla_{\mu_{n-1}} f(\mu_{n-1}, t_n) \cdot \sigma_{n-1} U_{n-1} + O(\sigma_{n-1}^2). \quad (59)$$

Multiplying (59) by $\frac{U_{n-1}}{\sigma_{n-1}}$ shows that $f(\mu_{n-1}, t_n) \cdot \frac{U_{n-1}}{\sigma_{n-1}}$ is the dominant exploding term. Its expectation is zero since U_{n-1} is centered Gaussian, so it can also be removed as a control variate:

$$\begin{aligned} \mathbb{E}_{z_{n-1}, z_n} \left[f(\mu_{n-1}, t_n) \cdot \frac{U_{n-1}}{\sigma_{n-1}} \right] &= \mathbb{E}_{z_{n-1}} \left[\frac{f(\mu_{n-1}, t_n)}{\sigma_{n-1}} \mathbb{E}_{z_n} [U_{n-1}] \right] = 0 \\ \Rightarrow \mathbb{E}_{z_{n-1}, z_n} \left[f(z_n, t_n) \cdot \frac{U_{n-1}}{\sigma_{n-1}} \right] &= \mathbb{E}_{z_{n-1}, z_n} \left[f(z_n, t_n) \cdot \frac{U_{n-1}}{\sigma_{n-1}} - f(\mu_{n-1}, t_n) \cdot \frac{U_{n-1}}{\sigma_{n-1}} \right] \\ &= \mathbb{E}_{z_{n-1}, z_n} \left[\frac{U_{n-1}}{\sigma_{n-1}} [f(z_n, t_n) - f(\mu_{n-1}, t_n)] \right]. \end{aligned} \quad (60)$$

Reinstating N in place of n as a random variable and substituting into (55) gives

$$\begin{aligned} &\text{CE}(q_\phi(z_0|x) \| p_\theta(z_0)) \\ &= H(q_\phi(z_{n_f})) + \frac{1}{2} \mathbb{E}_{N, z_N} [g^2(t_N) \| s_\theta(z_N, t_N) \|_2^2] \\ &\quad + \mathbb{E}_N \left[g^2(t_N) \mathbb{E}_{z_{N-1}, z_N} \left[\frac{U_{N-1}}{\sigma_{N-1}} \cdot [s_\theta(z_N, t_N) - s_\theta(\mu_{N-1}, t_N)] \right] \right] \\ &\quad - \mathbb{E}_N \left[\mathbb{E}_{z_{N-1}, z_N} \left[\frac{U_{N-1}}{\sigma_{N-1}} [f(z_N, t_N) - f(\mu_{N-1}, t_N)] \right] \right], \end{aligned} \quad (61)$$

where the random variable N is uniformly distributed on $\{1, \dots, n_f\}$. This concludes the proof. \square

C NVAE Architecture

The NVAE architecture in our experiments is the simplified version of the one implemented in [24]. We still set the number of latent scales to 1 and the number of groups of latent variables in this only latent scale to 2. We change the number of channels of the latent variables in each group from 20 to 1. We change the number of channels of the output feature representation of the initial convolution layer from 64 to 16. Such changes lead to a much simpler network, with the number of trainable parameters drastically reduced from 3,005,822 to 207,648.

C.1 Input

A batch of samples from the MNIST dataset is first zero-padded to obtain a $B \times 1 \times 32 \times 32$ feature, where B is the batch size. This feature is then passed to a 3×3 convolutional layer with padding of 1 and bias, which outputs a $B \times 16 \times 32 \times 32$ feature.

C.2 Preprocess Block

The preprocess block contains 6 cells. Each cell is based on the residual cell introduced in [23]. The input is passed to a batch normalization (BN) layer, activated by the Swish activation function [18] and passed to a 3×3 convolutional layer. The output goes through the same process again and is passed to a squeeze and excitation (SE) layer [11]. The first convolutional layer in the third cell has stride of 2 and outputs a $B \times 32 \times 16 \times 16$ feature. The first convolutional layer in the final cell has stride of 2 and outputs a $B \times 32 \times 8 \times 8$ feature. All six cells extend the residual connection to skip connection with coefficient 0.1.

C.3 Encoder Tower

The encoder tower contains 2 cells. Each cell has the same architecture as the cells in the preprocess block with stride of 1. The output of the first cell is a $B \times 32 \times 8 \times 8$ feature and is passed to both the second cell and the encoder combiner in the decoder tower. The output of the second cell is also a $B \times 32 \times 8 \times 8$ feature and is passed to the normal sampler.

C.4 Normal Sampler

The purpose of the normal sampler is to sample from the normal distribution. The output of the second cell in the encoder tower is activated by the ELU activation function [5] and passed to a convolutional layer. The output is a $B \times 2 \times 8 \times 8$ feature, which is splitted into two $B \times 1 \times 8 \times 8$ features and used as the mean and covariance of a normal distribution. A sample is generated from this distribution and passed to a convolutional layer to obtain a $B \times 1 \times 8 \times 8$ feature. This feature is then passed to the first decoder combiner in the decoder tower.

The whole process above is repeated for the output of the encoder combiner in the decoder tower. The output feature is then passed to the second decoder combiner in the decoder tower. There is also a $B \times 1 \times 8 \times 8$ sample from a normal distribution. This sample and the sample in the process above are concatenated as a $B \times 2 \times 8 \times 8$ feature, which is viewed as a batch of latent variables in the latent space determined by the encoder of this NVAE.

C.5 Decoder Tower

The decoder tower contains 2 cells. Each cell is modified from the residual cell. The $\text{BN} \rightarrow \text{Swish activation} \rightarrow \text{convolution}$ is replaced by the $\text{convolution} \rightarrow \text{BN} \rightarrow \text{Swish activation}$. An extra BN is added at the beginning. An extra $\text{convolution} \rightarrow \text{BN}$ is added before the final SE layer. The decoder tower also contains one encoder combiner and two decoder combiners. The first decoder combiner takes the output of the normal sampler and a $32 \times 8 \times 8$ learnable parameter as inputs. It outputs a $B \times 32 \times 8 \times 8$ feature, which is passed to the first cell in the decoder tower. The encoder combiner takes the outputs of the first cells in both the encoder tower and the decoder tower as inputs. The output is passed to the normal sampler. The normal sampler’s output and the first cell’s output are then passed to the second decoder combiner. Finally, the decoder combiner’s output is passed to the second cell. The output $B \times 32 \times 8 \times 8$ feature is passed to the postprocess block.

C.6 Postprocess Block

The postprocess block contains 6 cells. Each cell has the same architecture as the cells in the decoder tower. The first convolutional layer in the first cell has stride of -1 and outputs a $B \times 32 \times 16 \times 16$ feature. The first convolutional layer in the third cell has stride of -1 and outputs a $B \times 16 \times 32 \times 32$ feature. This output is obtained by skip connection, the same as the preprocess block.

C.7 Output

The output of the postprocess block is activated by the ELU function and passed to a 3×3 convolution layer. The output is a $B \times 1 \times 32 \times 32$ feature, which can be viewed as logits. The Bernoulli distribution determined by the logits can be viewed as the output of the decoder of this NVAE.

D Experiment Results

Table 3: Low data MNIST ($N = 3000$)

model	FID (\downarrow)	IS (\uparrow)
LSGM	27.1	9.12
LNDSM-SGM	15.0	9.57

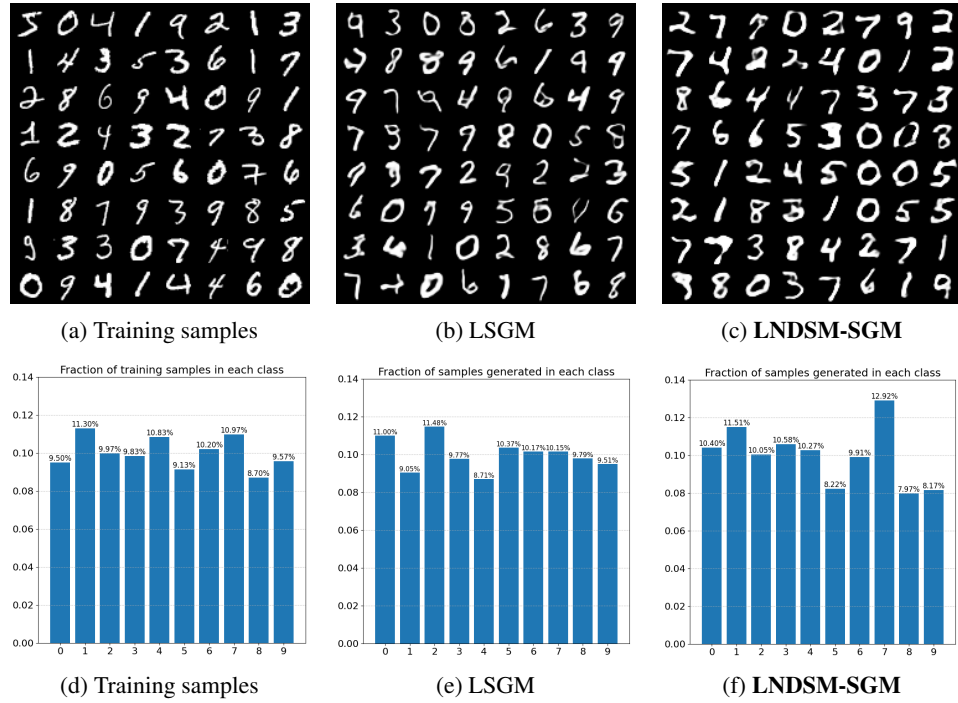


Figure 2: LSGM and LNDSM-SGM trained using the low data MNIST dataset. (a) and (d): Snapshot and fraction of different digits of the training samples. (b) and (e): Snapshot and fraction of different digits of the 10,000 samples generated by the LSGM. The KL divergence from the fraction of the training samples to the fraction of the generated samples: 0.00883. (c) and (f): Snapshot and fraction of different digits of the 10,000 samples generated by the LNDSM-SGM. The KL divergence from the fraction of the training samples to the fraction of the generated samples: 0.00439.

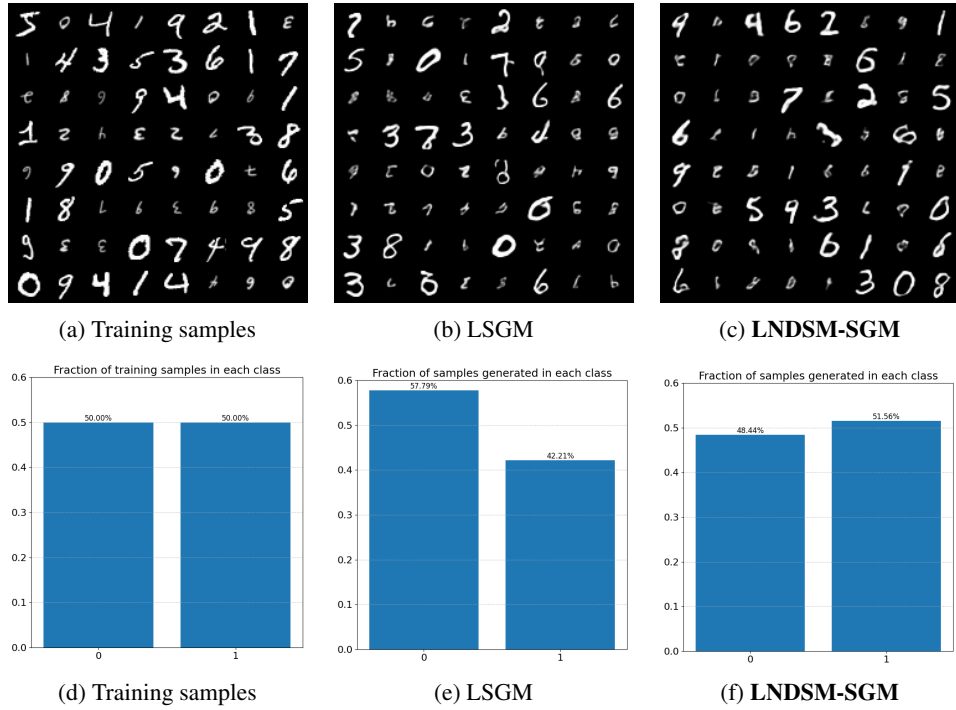


Figure 3: LSGM and LNDSM-SGM trained using the full Approx.-C2-MNIST dataset. (a) and (d): Snapshot and fraction of different digits of the training samples. (b) and (e): Snapshot and fraction of different digits of the 10,000 samples generated by the LSGM. (c) and (f): Snapshot and fraction of different digits of the 10,000 samples generated by the LNDSM-SGM.